# Limits to the extraction of information from multi-hop skywave radar signals

Stuart Anderson

*Abstract*— **The performance of HF skywave radar systems is customarily referred to in terms of single-hop propagation, a mechanism which provides illumination of the earth's surface out to ranges of around 4000 kilometres. In practice, the process of ionospheric reflection often supports multiple hops, though the signals are inevitably subjected to much greater distortion and contamination. In this paper we address the issue of adequacy of conventional models of multi-hop propagation. We formulate a detailed model which accounts for intermediate surface scattering, and obtain a representation in terms of integrals in $\vec{x} - \vec{k}$ space. We proceeed to evaluate the resulting expressions for several cases of interest. The results demonstrate that it is vital to understand the complexities of multi-hop propagation if this method of observation is to be exploited for remote sensing of the ocean at extreme ranges.**

*Keywords*—**HF radar, remote sensing, ionosphere, radiowave propagation**

## I. Introduction

HF skywave 'over-the-horizon' radar (OTHR) exploits the reflection of radiowaves by the ionosphere to illuminate the distant earth's surface, thereby providing a means for detecting and tracking aircraft and ships at ranges up to several thousand kilometres. In addition, information about the sea surface geometry and dynamics is embedded in the radar echoes, and this information can be manipulated to yield estimates of a variety of oceanographic and meteorological parameters such as significant waveheight and wind velocity [1]. Of course, the vast coverage achieved by OTHR is obtained at the expense of subjecting the signals to the vagaries of the ionospheric medium, leading to distortion and contamination which often degrades the extracted information [2].

The zone illuminated by radar emissions which have undergone a single reflection from the ionosphere extends typically from a minimum range ('skip' distance) of about 1000 km to a maximum of around 4000 km, and for most purposes this constitutes an upper bound to the range of observability of echoes of interest. Nevertheless, it is evident that signals scattered from the earth's surface in the 'one-hop' zone may undergo a second forward ionospheric reflection to illuminate more distant regions, and so on.

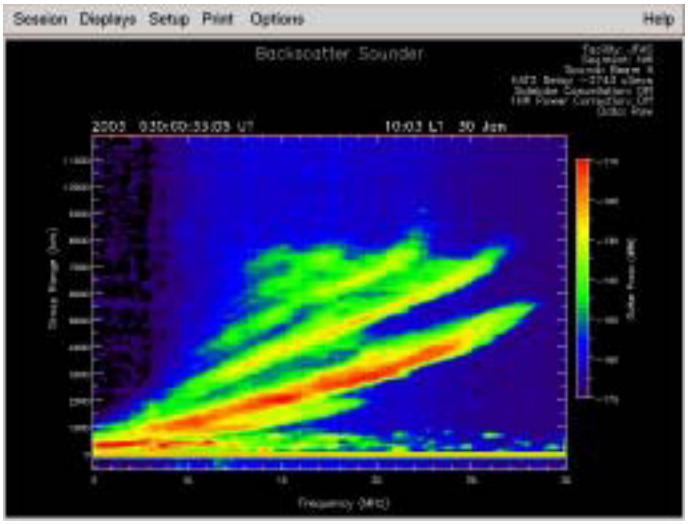


Fig. 1. Backscatter ionogram showing one-, two- and three-hop modes

Figure 1 shows a backscatter ionogram in which one-, two- and three-hop echoes are apparent. Ray-tracing codes can be used to model these multi-hop paths, as illustrated in figure 2, which was generated with a two-dimensional code which employs the modified Haselgrove equations to compute the eikonal rays through a model ionosphere, plotting the resulting trajectories in the range-height plane.

Echoes received via these multi-hop propagation paths may, in principle, be analysed to provide oceanographic information out to ranges in excess of 6000 km, noting that the geometric spreading associated with the diverging radar beams results in very coarse spatial resolution at long ranges. Of course, the increase in size of the radar resolution cells means that the clutter power increases proportionately, so, unlike echoes from discrete targets, the clutter returns may decay relatively slowly with range and hence may maintain the clutter-to-noise ratio at a level able to support analysis. On the other hand, the additional transits through the ionosphere cause further degra-

# Report Documentation Page

*Form Approved*
*OMB No. 0704-0188*



| 1. REPORT DATE | 2. REPORT TYPE | 3. DATES COVERED |
|---|---|---|
| **14 APR 2005** | **N/A** | **-** |

| 4. TITLE AND SUBTITLE | 5a. CONTRACT NUMBER |
|---|---|
| **Limits to the extraction of information from multi-hop skywave radar signals** | 5b. GRANT NUMBER |
| | 5c. PROGRAM ELEMENT NUMBER |
| 6. AUTHOR(S) | 5d. PROJECT NUMBER |
| | 5e. TASK NUMBER |
| | 5f. WORK UNIT NUMBER |
| 7. PERFORMING ORGANIZATION NAME(S) AND ADDRESS(ES) **Intelligence, Surveillance & Reconnaissance Division, Defence Science and Technology Organisation Salisbury, SA 5108 Australia** | 8. PERFORMING ORGANIZATION REPORT NUMBER |
| 9. SPONSORING/MONITORING AGENCY NAME(S) AND ADDRESS(ES) | 10. SPONSOR/MONITOR'S ACRONYM(S) |
| | 11. SPONSOR/MONITOR'S REPORT NUMBER(S) |

12. DISTRIBUTION/AVAILABILITY STATEMENT
**Approved for public release, distribution unlimited**

13. SUPPLEMENTARY NOTES
**See also ADM001798, Proceedings of the International Conference on Radar (RADAR 2003) Held in Adelaide, Australia on 3-5 September 2003., The original document contains color images.**

14. ABSTRACT

15. SUBJECT TERMS

| 16. SECURITY CLASSIFICATION OF: | | | 17. LIMITATION OF ABSTRACT | 18. NUMBER OF PAGES | 19a. NAME OF RESPONSIBLE PERSON |
|---|---|---|---|---|---|
| a. REPORT | b. ABSTRACT | c. THIS PAGE | | | |
| **unclassified** | **unclassified** | **unclassified** | **UU** | **7** | |

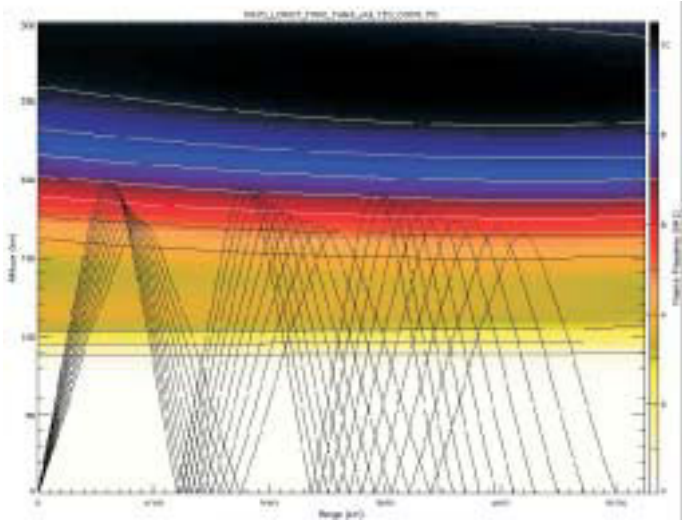

Fig. 2. Ray fan computed for a model ionosphere, showing multihop modes

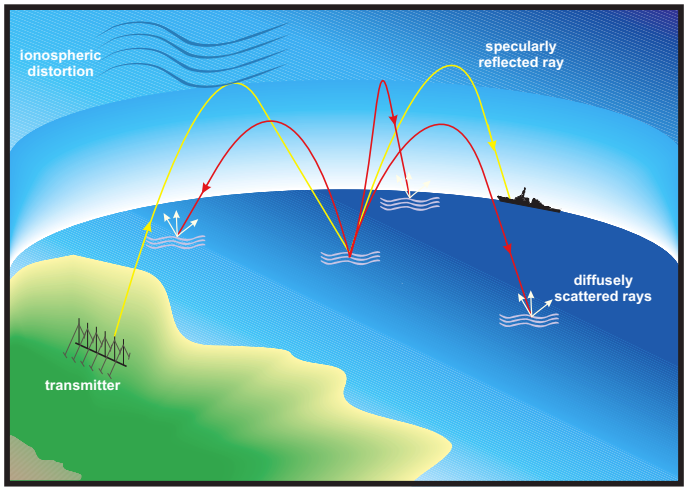


Fig. 3. Schematic showing the progressive diffusion of the transmitted rays on successive ground reflections

dation of the signal, so the availability of exploitable echoes is reduced.

In view of these factors, it is often held that, under clement propagation conditions, the exploitation of multi-hop echoes can proceed in a manner similar to that employed for one-hop echoes, using essentially the same algorithms for parameter extraction. It is the purpose of this paper to demonstrate that the situation is more complex than appears at first sight, and that analysis of multi-hop echoes demands a more sophisticated model of the radar observation process.

## II. The radar process model for multi-hop propagation

### A. General formulation

The process model equation for simple one-hop propagation can be written [3]

$$s = \tilde{P}\tilde{R}\tilde{M}_S^R\tilde{S}\tilde{M}_T^S\tilde{T}w + \tilde{P}\tilde{R}\tilde{M}_N^R n + m \qquad (1)$$

where

$w$ represents the selected waveform

$\tilde{T}$ represents the transmitting complex, including transmitters and antennas

$\tilde{M}_T^S$ represents propagation from transmitter to target scattering region

$\tilde{S}$ represents all scattering processes in the target region

$\tilde{M}_S^R$ represents propagation from target scattering region to receiver

$n$ represents an external noise source

$\tilde{M}_S^R$ represents propagation from noise source to receiver

$m$ represents internal noise

$\tilde{R}$ represents the receiving complex, including antennas and receivers

$\tilde{P}$ represents the signal processing

$s$ represents the signal decomposition after processing

The general form of the extension to the multi-hop propagation case can be written as a sum over orders of hop. Immediately we observe that the process must account for scattering from areas far removed from the great circle path; this is illustrated schematically in figure 3.

It will be convenient in what follows to refer on occasion to the number of ground bounces, rather than the number of ionospheric hops, particularly to facilitate description of non-reciprocal paths. The process model is then written :

$$\begin{aligned} s &= \tilde{P}\sum_{n_B=1}^{N}\tilde{R}[\prod_{b=1}^{n_B}\tilde{M}_{S(b)}^{S(b+1)}\tilde{S}(b)]\tilde{M}_T^{S(1)}\tilde{T}w \qquad (2)\\ &+ \sum_{n_B=1}^{N}\tilde{R}[\prod_{b=1}^{m_B}\tilde{M}_{S(b)}^{S(b+1)}\tilde{S}(b)]\tilde{M}_N^{S(1)}n + m \end{aligned}$$

Depending on the spatial filtering properties of the operators $\tilde{T}$, $\tilde{M}$, $\tilde{R}$ and $\tilde{P}$, some of these terms may be suppressed. Spatial filtering implemented in the signal processing operator $\tilde{P}$ will suppress echoes arriving from directions other than those belonging to the subspace defined by the array steering vector. Additional spatial filtering in the vertical plane arises from (i) the elevation radiation patterns of the antenna elements,

embedded in the transmit and receive operators $\tilde{T}$ and $\tilde{R}$, each of which defines an intensity/sensitivity distribution on the base of the ionosphere, and (ii) the propagation operators $\tilde{M}$, which incorporate the refractive properties of the ionosphere and hence account for focussing and defocussing. Together, these factors usually render some terms in the expansion insignificant, though for specific applications one may need to verify this.

### *B. Explicit representation of the operators*

In order to proceed with calculations, we need to choose an explicit mathematical representation for the operators. The choice depends on the physical domain in which the radar process is to be studied. For example, if the transformation of the polarisation state of the signal were the only feature of interest, the analysis could be carried out using the Jones calculus.

It is natural and convenient to adopt a representation based on integrals over the space and wavevector variables; for the present we shall suppress the (evolving) polarisation state of the field and the temporal dependence of the operators.

We can then write, to second order :

$$\tilde{T} = \frac{1}{4\pi} P_T G_T(\vec{k})(.) \tag{3}$$

$$\tilde{M}_{\vec{r}}^{\vec{r}'} = \int d\vec{k}\, G(\vec{k}', \vec{r}', \vec{k}, \vec{r})(.) \tag{4}$$

$$\begin{aligned} \tilde{S} &= \int d\vec{k}\delta(\vec{k}' - \vec{k}'.\hat{n} - \vec{k} + \vec{k}.\hat{n})\delta(\vec{k}'.\hat{n} + \vec{k}.\hat{n})(.) \\ &+ \int d\vec{\kappa}_1 F^{(1)}(\vec{k}_i, \vec{k}_s, \vec{\kappa}_1) S(\vec{\kappa}_1)(.) \\ &+ \int\int d\vec{\kappa}_1 d\vec{\kappa}_2 F^{(2)}(\vec{k}_i, \vec{k}_s, \vec{\kappa}_1, \vec{\kappa}_2) S(\vec{\kappa}_1) S(\vec{\kappa}_2)(.) \end{aligned} \tag{5}$$

$$\tilde{R} = \frac{1}{4\pi} G_R(\vec{k})(.) \tag{6}$$

where $G(\vec{k}', \vec{r}', \vec{k}, \vec{r})$ is the Green's function for skywave propagation and $S(\vec{\kappa})$ denotes the directional wave spectrum of the sea surface. $F^1(\vec{k_i}, \vec{k_s}, \vec{\kappa_1})$ and $F^2(\vec{k_i}, \vec{k_s}, \vec{\kappa_1}, \vec{\kappa_2})$ denote the kernels for the first and second order scattering respectively.

### *C. Construction of the model for two-hop propagation*

The generality of the formal model enables it to incorporate diverse effects including dispersion, generalised Faraday rotation, tilts and ionospheric disturbances and so on. Our focus here is on the relative importance of various contributions to the received field,

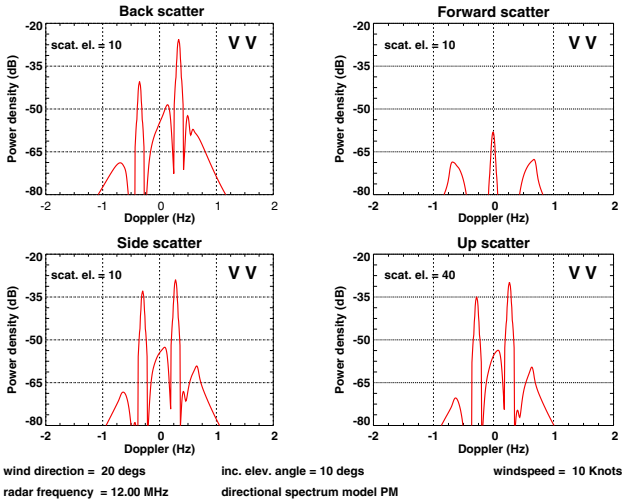


Fig. 4. Theoretical Doppler spectra of sea clutter for various categories of scattering geometry

so we shall simplify the physics as much as possible without compromising the essential aspects. This has the advantage of speeding up the calculations - on a 2GHz Pentium PC, the model can track 400,000 rays in about 10 minutes.

For the computations reported here, we adopt a spherical earth, a concentric spherical mirror as our ionosphere, consider only the zeroth and first order terms in the expansion for the sea scatter, assume a land-free ocean, and choose a transmit antenna pattern with uniform sector gain in both the vertical and horizontal planes. Receive beams are formed over 360° assuming element patterns isotropic in azimuth with uniform sector gain in elevation. Array beamwidth is, naturally, a function of azimuth. The sea surface is assumed to be fully-developed over the frequency band corresponding to the Bragg resonant scattering mechanism, and isotropic in azimuth.

Ultimately the distribution of energy in the Doppler domain is of central interest, so it is important to model the scattering from the sea surface with adequate fidelity. For this purpose we employ the *JINSCAT* code developed in DSTO for remote sensing and ship detection applications. Representative spectra computed with *JINSCAT* for several broad classes of scattering geometry are shown in figure 4.

While the full Doppler spectrum can be computed in an accurate and natural way with our model, the present paper restricts attention to the total power, without a decomposition in Doppler. As shown below, it turns out that computing just the power suffices to answer the key questions posed here; results generated for the higher-dimensional analysis will be published

elsewhere. A further restriction imposed here is to assume collocated transmit and receive antennas; this is done simply to facilitate comparison with common experience - the model is equally applicable to arbitrary bistatic geometries [4].

We shall consider the case of a radar employing two uniform linear arrays, a transmitting array $10\ \lambda$ in length and a receiving array $100\lambda$ in length. For a specified ionospheric height h, and a take-off elevation angle $\theta$ from point $\vec{r}$, the ground and slant ranges to the ground bounce point $\vec{r}'$ are given by :

$$\alpha = \frac{Re * sin(\frac{\pi}{2} + \theta)}{R_e + h} \quad (7)$$

$$\beta = \frac{\pi}{2} - \theta - \arcsin(\alpha) \quad (8)$$

$$R_{gr} = 2 * R_e * \beta \quad (9)$$

$$R_{sl} = 2 * R_e * \frac{sin\beta}{\alpha} \quad (10)$$

where $R_e$ is the radius of the earth . It is convenient to employ a mixed coordinate system, wherein $\vec{k}$ is defined relative to the local normal $\hat{n}$ at $\vec{r}$, while $\vec{k}'$ is defined relative to the local normal $\hat{n}'$ at $\vec{r}'$. This facilitates the calculation when the surface scattering is the primary object of study.

The Green's function then takes the form

$$G(\vec{k}', \vec{r}', \vec{k}, \vec{r}) = \frac{exp(ikR_{sl})}{R_{sl}} \delta(k' - k) \delta(\vec{k}'.\hat{n}' + \vec{k}.\hat{n}) \quad (11)$$

We note that most of the process model operators depend on elevation angle, including not only the antenna patterns but also the scattering from the terrestrial surface. As shown in Figure 5, the elevation angles of one-and two-hop modes can be very different at a given range, which can lead to substantial changes in the scattering coefficient when the Bragg frequency is close to the wave spectrum peak.

## III. Coordinate registration for multi-hop propagation

The visual appearance of the backscatter ionogram presented in figure 6 suggests that the two-hop mode extends the range coverage from the one-hop limit at 3500 km to a new maximum of about 5500 km. This is not strictly correct - the Y-axis in the figures 1 and 6 is the 'group' or 'slant' range, and the conversion to ground range must take account of the actual propagation path. In the case of two-hop modes, the additional distance travelled in the course of undergoing two ionospheric reflections must be taken into account. The relevant relationships and corrections are presented in figures 7 - 9. Figure 7 plots the slant (group) range as a function of ground range, parametrised by ionospheric height, for both one- and two-hop propagation. This information can be used to calculate the two-hop range correction factor, as presented in Figure 8, which shows the range difference of two-hop as opposed to one-hop propagation to a given range. Here and in all figures, the horizon for a given ray is indicated by termination of the corresponding curve. Finally, it is useful to plot one mode against the other, as is done in Figure 9, to emphasise the relative (as opposed to the absolute) range discrepancy.

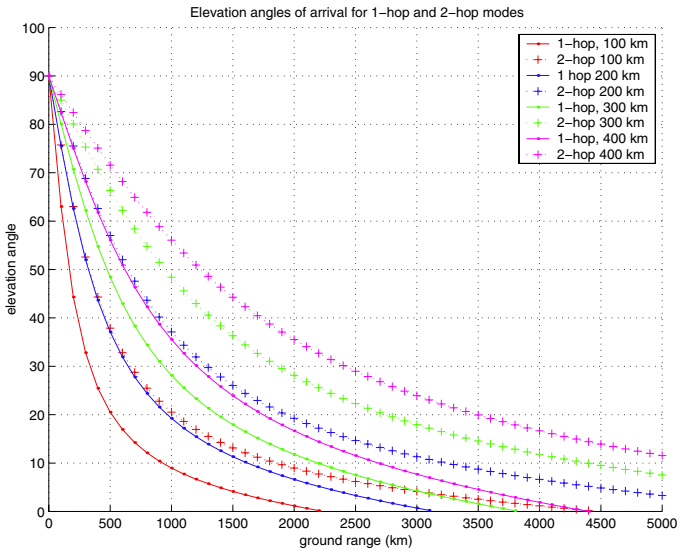


Fig. 5. Variation of elevation angle with ground range for one- and two-hop modes

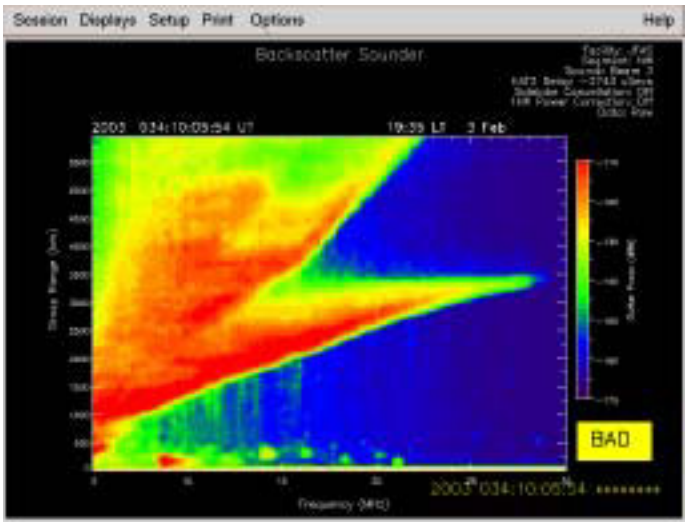


Fig. 6. Backscatter ionogram showing the transition from the one-hop regime to the two-hop regime

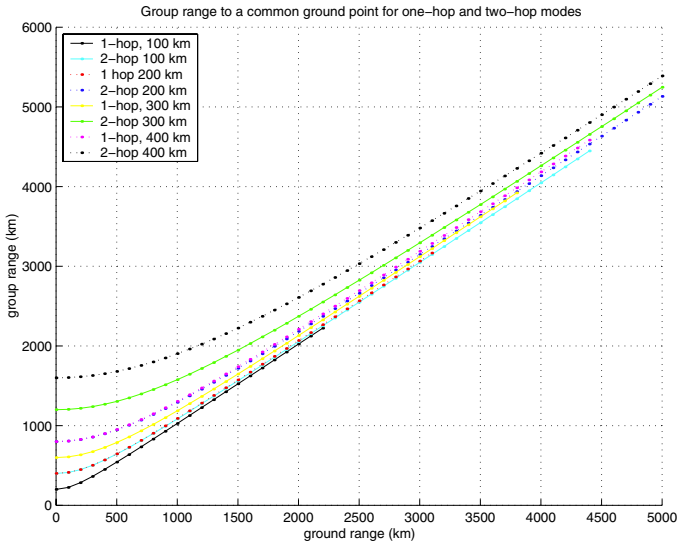


Fig. 7. Comparison of group ranges for one-hop and two-hop propagation to a given ground range

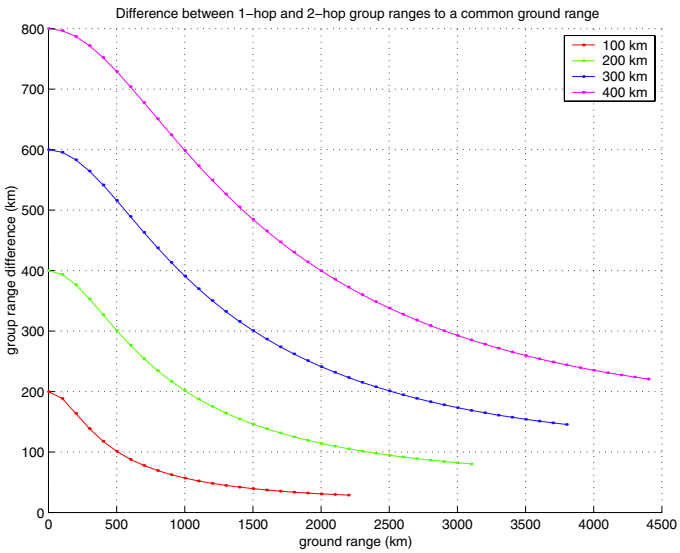


Fig. 8. The range difference introduced by two-hop propagation as opposed to one-hop propagation

## IV. Climatology of multi-hop propagation

The Jindalee radar frequency management system records backscatter ionograms routinely, twenty four hours a day, and has done so since 1982 with some short interruptions. Until 1999 the data was acquired one beam at a time (there are eight beams spanning the 90 deg arc to the north-west of Australia) but since July 1999, when an eight-channel receiver was fitted, all beams have been collected simultaneously. Typically the full set of ionograms is updated every 4 minutes, covering ranges out to 12,000 kilometres.

This extensive database is ideally suited to the statistical analysis of the directional, diurnal, seasonal

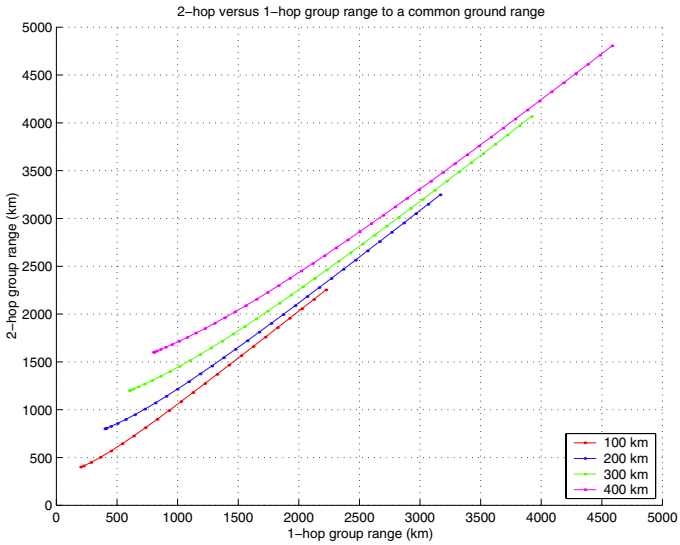


Fig. 9. Group ranges compared : two-hop versus one-hop

and sunspot number dependence of multihop propagation. Such an analysis lies beyond the scope of the present paper, but we note in passing that in preparing this paper we examined a single month's data in some detail and identified distinct patterns in multihop coverage.

## V. Results

The first property of interest is the extent of the spread in azimuth of the radar echoes after diffuse scattering from the first bounce footprint. Figure 10 shows a histogram of azimuthal angle-of-arrival of $10^5$ rays originally transmitted in a broad beam of full width 120° centred on 270°. It is apparent that the tendency is for considerable broadening but with the distribution centred around the axis of the transmitted beam. This is a consequence of the fact that the diffusely-scattered rays are generated with a uniform distribution in azimuth from the first bounce point onwards. Note that this figure reflects only the angle-of-arrival of the rays, not their amplitudes.

The key issue is the magnitude of the contribution from the diffusely-scattered field relative to that of the specularly scattered field. It is appropriate to use a common scale when presenting range-Doppler maps of the synthesised receiver output, and this was first implemented by using the global maximum over the families of specularly-reflected and diffusely-scattered triple-bounce modes. Later an alternative approach was adopted - we included in the output the returns arriving via singly-scattered one-hop propagation, and used the global maximum over all three families as the scaling constant. This approach facilitates a com-

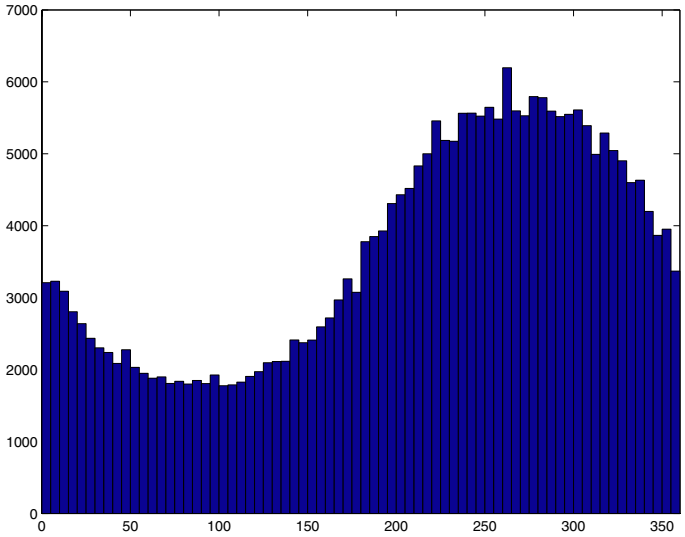


Fig. 10. A histogram of azimuthal angle-of-arrival at the receiving array for triple-bounce diffusely-scattered multihop rays

parison between one-hop and two-hop specularly reflected echoes. An example of a 'triptych' display of the range-Doppler maps for the three families of rays is shown in Figure 11. For ease of interpretation, only 10 transmitted rays are shown, with each yielding a single received ray for the non-diffusely scattered modes. In contrast, the diffusely-scattered rays spread more or less uniformly over a substantial range extent.

The relative magnitude of the diffusely-scattered received field relative to the specularly reflected two-hop return is seen to be around -30 dB for the assumed parameter values. This contribution would fall below the subdominant Bragg line on almost all realisations of the sea clutter Doppler spectrum, but is certainly comparable with much of the second-order clutter spectrum. It is the latter which is central to the extraction of most of the detailed sea state information sought in HF radar remote sensing.

## VI. Conclusion

We have developed a computational model able to compute the contributions of diffusely-scattered fields arising from non-specular reflection (bistatic scattering) at the ground reflection points for multiple-hop propagation paths. The significance of these echoes is determined by their magnitude relative to the echoes received via specular reflection at the bounce points, and by their spectral content.

Early calculations reveal that the diffusely-scattered returns lie $30dB$ below the specularly-reflected returns for the two-hop propagation case. This results has important implications for remote sensing :

(a) under conditions corresponding to the assumed parameter values, the diffusely-scattered returns are not so strong as to bias the Bragg line ratio appreciably, so information such as wind direction estimated from the Bragg line ratio should not be affected

(b) procedures for estimating sea state and other ocean surface characteristics, including inversion to yield the full directional wave spectrum, may be seriously corrupted by the presence of diffuse multi-hop contributions

(c) the relative magnitude of the diffusely-scattered contributions is strongly influenced by the antenna patterns, both transmit and receive, with obvious implications for radar design

(d) the contributions from different areas will, in general, have experienced different phase path modulations as a consequence of the spatial and temporal variability of the ionosphere, leading to additional contamination of the desired Doppler spectra

(e) the prospect of reliable remote sensing at extreme ranges via multi-hop propagation will depend on the development of new techniques able to detect, estimate and perhaps even compensate for diffuse scattering contamination.

Acknowledgment

It is a pleasure to acknowledge the assistance of Mr James Morris who made many helpful suggestions for improving the efficiency of the *MULTIHOP* code.

## VII. References

Anderson, S.J., 'Remote Sensing with the JINDALEE Skywave Radar (Invited paper), IEEE Journal of Oceanic Engineering, Vol. OE-11, pp.158-163, April 1986

Anderson, S.J., and Abramovich, Y.I., 'A unified approach to detection, classification and correction of ionospheric distortion in HF skywave radar systems', Radio Science, Vol.33, No.4, pp.1055-1067, July-August 1998

Anderson, S.J., 'Stereoscopic and Bistatic Skywave Radars : Assessment of Capabilities and Limitations', Proceedings of Radarcon-90, Adelaide, Australia, pp.305-313, April 1990

Anderson, S.J., 'The Challenge of Signal Processing for HF Over-the-Horizon Radar', Proceedings of the Workshop on Signal Processing and Applications, WOSPA'93, Brisbane, Australia, December 1993

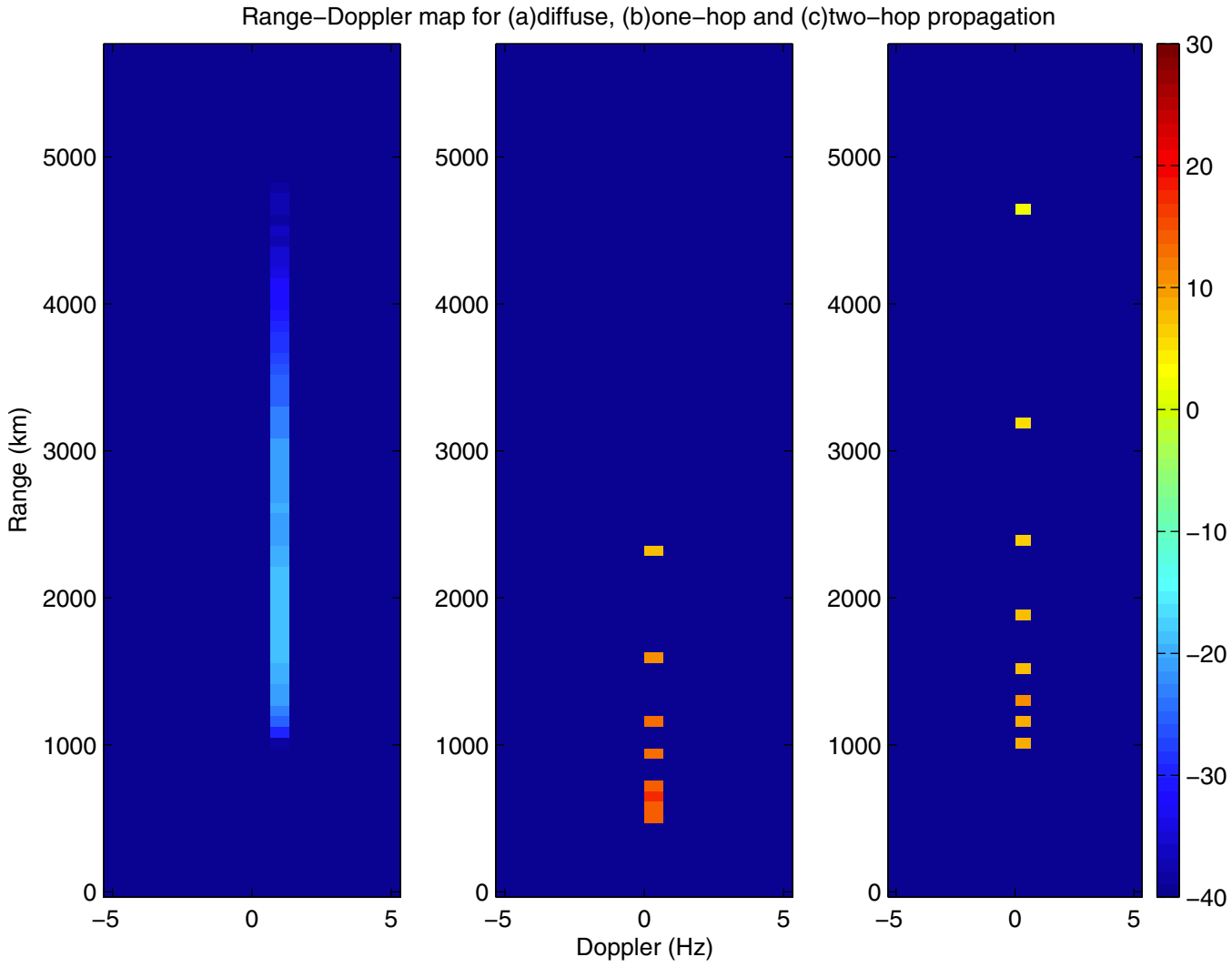


Fig. 11. Range-Doppler maps computed for : (a) diffusely-scattered triple-bounce rays, (b) singly-scattered rays (backscatter), and (c) specularly-scattered triple-bounce (two-hop) rays